Iraqi Journal of Physics, 2020 *Vol.18, No.46, PP. 29-38*

DOI: 10.30723/ijp.18.46.29-38

Study of the nuclear structure of halo nuclei ^{23}O and ^{24}F using the two-body model

Ghufran M. Sallh, Ahmed N. Abdullah

Department of Physics, College of Science, University of Baghdad, Baghdad, Iraq

Corresponding author: ghufranmahdy@yahoo.com

Abstract

The nuclear structure including the matter, proton and neutron densities of the ground state, the nuclear root-mean-square (rms) radii and elastic form factors of one neutron ^{23}O and ^{24}F halo nuclei was studied by the two body model of $(core + n)$ within the harmonic oscillator (HO) and Woods-Saxon (WS) radial wave functions. The calculated results show that the two body model within the HO and WS radial wave functions succeed in reproducing neutron halo in these exotic nuclei. Moreover, the Glauber model at high energy was used to calculate the rms radii and reaction cross section of these nuclei. The calculated results were compared with the experimental data.

Key words

Halo nuclei, root mean square radii, Glauber model.

Article info.

Received: Jun. 2020
Accepted: Aug. 2020
Published: Sep. 2020

دراسة التركيب النووي لنوى الهالة ^{23}O و ^{24}F باستخدام أنموذج الجسيمين

غفران مهدي صالح، أحمد نجم عبدالله

قسم الفيزياء، كلية العلوم، جامعة بغداد، بغداد، العراق

الخلاصة

تم دراسة التركيب النووي مثل توزيعات الكثافة الكتلية، البروتونية و النيوترونية وانصاف الاقطار النووية وعوامل التشكل لنوى ^{23}O و^{24}F باستخدام أنموذج الجسيمين مع الدوال الموجية لجهدي المتذبذب التوافقي وودز- ساكسون. وفقا للنتائج المحسوبة وجد ان هذا الانموذج يعطي وصفاً جيدا للتركيب النووي لنوى الهالة تحت الدراسة. كما تم استخدام نموذج جلوبر عند الطاقات العالية لدراسة المقاطع العرضية للتفاعل وانصاف النووية لهذه النوى. وتمت مقارنة النتائج مع القيم العملية.

Introduction

One of the most exciting discoveries in the recent experimental progress using radioactive nuclear beams is the neutron halo in some light neutron-rich nuclei [1, 2]. On the other hand, the search for proton halo in light proton-rich nuclei has attracted much attention in recent years. The theory based on the relativistic mean filed (RMF) approximation predicts the existence of proton halo or proton skin structure in some proton-rich nuclei [3, 4] and experiments have subsequently observed some of the theoretical predictions [5, 6].

The observed neutron halo nuclei, such as ^{11}Li, ^{11}Be, ^{14}Be and ^{17}B, are in their ground state and are located near the drip line. In principle, the neutron halo appears in very loosely bound nuclear system with a low density which results in substantially large spatial extension of the wave function for the neutron (proton) halo in these nuclei [7].

It is well known that Glauber model analysis on reaction cross section is an important and feasible tool to deduce

the nuclear size, which directly connects the reaction cross section to the nuclear density distribution. The Glauber theory in the optical limit (OL) approach has been successfully applied to describe unstable nucleus-nucleus scattering [8].

A. Alsajjad and Abdullah [9] used Woods-Saxon (WS) and Harmonic Oscillator (HO) potentials wave functions within the two-body model of [$Core+p(n)$] to study the ground state features such as the neutron, proton and matter densities, the associated root mean square (rms) radii and the elastic form factors of exotic ^{17}F and ^{19}C nuclei. According to the calculated results, it was found that this model provides a good description on the nuclear structure of the above exotic nuclei. The reaction cross sections for these nuclei have been studied using the Glauber model with an optical limit approximation (OLA) at high energy region. Abdullah [10] studied the ground state densities of halo ^{6}He, ^{11}Li, ^{12}Be and ^{14}Be nuclei using a three-body model of (core + *n* + *n*). The long tail property was shown in the calculated neutron and matter densities of these nuclei. The calculated results of matter densities were in good accordance with the experimental results. Abdullah [11] used the two body model of (Core+n) within the radial wave functions of the cosh potential to investigate the ground state features such as the proton, neutron and matter densities, the rms nuclear proton, neutron, charge and mass radii of unstable neutron-rich ^{14}B, ^{15}C, ^{19}C and ^{22}N nuclei. The calculated results showed that the two body model with the radial wave functions of the cosh potential succeeds in reproducing neutron halo in these nuclei.

Abdullah [12] used the radial wave functions of the Bear–Hodgson potential to study the ground state features such as the proton, neutron and matter densities and the associated rms radii of two neutrons halo ^{6}He, ^{11}Li, ^{14}Be and ^{17}B nuclei. These halo nuclei were treated as a three-body system composed of core and outer two-neutron (Core + n + n). The radial wave functions of the Bear–Hodgson potential were used to describe the core and halo density distributions. The interaction of core-neutron takes the Bear–Hodgson potential form. The outer two neutrons of ^{6}He and ^{11}Li interact by the realistic interaction REWIL whereas those of ^{14}Be and ^{17}B interact by the realistic interaction of HASP. The obtained results showed that this model succeeds in reproducing the neutron halo in these nuclei. Elastic charge form factors for these halo nuclei were analyzed via the plane wave Born approximation.

In this work, the WS and HO potentials wave functions will be used within the two-body model of $(core + n)$ to study the nuclear structure including the matter, proton and neutron densities of the ground state, the nuclear root-mean-square (rms) radii and elastic form factors of one neutron ^{23}O and ^{24}F halo nuclei. Moreover, the Glauber model with an OLA will be used to calculate the rms radii and the σ_R of these nuclei.

Theory

The distributions of matter density for unstable exotic nuclei are given as [11]:

$$\rho_m(r) = \rho_c(r) + \rho_v(r) \qquad (1)$$

where $\rho_c(r)$ and $\rho_v(r)$ are the core and halo densities, respectively and can be written as [12]:

$$\rho_c(r) = \frac{1}{4\pi}\sum_{n\ell} X_c^{n\ell} \, |R_{n\ell}(r)|^2 \qquad (2)$$

$$\rho_v(r) = \frac{1}{4\pi} X_v^{n\ell} |R_{n\ell}(r)|^2 \qquad (3)$$

where $X_{c(v)}^{n\ell}$ refer to proton or neutron number in the sub-shell $n\ell j$ and $R_{n\ell j}(r)$ is the radial wave function.
The distributions of matter density in Eq.(1) can be written in terms of proton $[\rho^p(r)]$ and neutron $[\rho^n(r)]$ densities as [10]:

$$\rho_m(r) = \rho^n(r) + \rho^p(r) \quad (4)$$

where $\rho^p(r)$ and $\rho^n(r)$ can be written as [10]:

$$\rho^g(r) = \rho_c^g(r) + \rho_v^g(r) \quad g \equiv p,n \quad (5)$$

In the present work, the calculated results are analyzed using two density parameterizations which are WS and HO.

In the WS parameterization, the core and halo densities are parameterized with WS radial wave function which are taken from the solution to the radial part of the Schrodinger equation using WS potential [10]:

$$\frac{\hbar^2}{2\,\mu}\frac{d^2R_{nlj}(r)}{dr^2} + \left[\varepsilon_{nlj} - V(r) - \frac{\hbar^2}{2\,\mu}\frac{\ell(\ell+1)}{r^2}\right]R_{nlj}(r) = 0 \quad (6)$$

where $\varepsilon_{n\ell j}$ is the single-particle energy, n, ℓ and j are the principle, orbital angular and total quantum numbers and μ is the reduced mass of the core and single nucleon $\mu = m(A-1/A)$, A is the nuclear mass number and m is the nucleon mass. The $V(r)$ is the potential of the core given as [13]:

$$V(r) = V_0(r) + V_{so}(r)\,L.S + V_c(r) \quad (7)$$

where $V_0(r)$ is the central potential that takes the form of WS potential [10]:

$$V_0(r) = \frac{-V_0}{1 + [e^{(r-R_0)/a_0}]} \quad (8)$$

V_0 is depth of central potential.
$V_{so}(r)$ is the spin-orbit potential expressed as [10]:

$$V_{so}(r) = V_{so}\frac{1}{r}\left[\frac{d}{dr}\frac{1}{(1+e^{(r-R_{so})/a_{so}})}\right] \quad (9)$$

V_{so}: is depth of spin-orbit potential, and $V_c(r)$: is the Coulomb potential (for protons only) generated by a homogeneous charged sphere of radius R_c [14]:

$$V_c(r) = \begin{cases} \frac{Ze^2}{r} & \text{for} \quad r > R_c \\ \frac{Ze^2}{R_c}\left[\frac{3}{2} - \frac{r^2}{2R_c^2}\right] & \text{for} \quad r \le R_c \end{cases}$$

and $V_c(r) = 0$ for neutrons (10)

In the HO parameterization, the core and halo densities are parameterized with harmonic oscillator radial wave function given by [15]:

$$R_{n\ell}(r) = \frac{1}{(2\ell+1)!!}\left[\frac{2^{\ell-n+3}(2n+2\ell-1)!!}{\sqrt{\pi}b^3(n-1)!}\right]\left(\frac{r}{b}\right)^{\ell} e^{-\frac{r^2}{2b^2}} \sum_{k=0}^{n-1}(-1)^k \frac{(n-1)!2^k(2\ell+1)!!}{(n-k-1)!k!(2\ell+2k+1)!!}\left(\frac{r}{b}\right)^{2k} \quad (11)$$

where $b = \sqrt{\hbar/M_p\omega}$ is the HO size parameter (which is the length parameter for the HO well), M_p is the mass of the proton and ω is the angular frequency.

The rms radii of the neutron and proton distributions can be calculated by [16]:

$$r_g = \langle r_g^2\rangle^{\frac{1}{2}} = \left[\frac{\int r^2\rho_g(r)dr}{\int \rho_g(r)dr}\right]^{\frac{1}{2}} \quad g = n,p \quad (12)$$

The elastic form factors in the plane wave Born approximation (PWBA) are written as [17]:

$$F(q) = \frac{4\pi}{Z}\int_0^{\infty} \rho_p(r)j_0(qr)r^2dr \quad (13)$$

where Z is the atomic number, $j_0(qr)$ the Bessel function and q the momentum transfer to the target nucleus from the incident electron.

The reaction cross section (σ_R) using the Glauber model within OLA is given by [18]:

$$\sigma_R = 2\pi\int [1 - T(b)]\,b\,db \quad (14)$$

where $T(b)$ is the transparency function at impact parameter b.
The $T(b)$ in OLA is given in terms of the elastic $S-$matrix for the projectile-target system as [19]:

$$T(b) = \left|S_{el}^{OL}(b)\right|^2 \quad (15)$$

Where

$$S_{el}^{OL}(b) = exp[iO_{PT}(b)] \quad (16)$$

$$O_{PT}(b) = \int_{-\infty}^{\infty} dR_3 \int d\vec{r}_1 \int d\vec{r}_2 \rho_P(r_1)\rho_T(r_2) f_{NN}\left(\left|\vec{R} + \vec{r}_1 - \vec{r}_2\right|\right) \quad (17)$$

$O_{PT}(b)$ is the overlap of the densities of ground state for target and projectile (ρ_T and ρ_P, respectively).

Results and discussion

The nuclear structure including the matter, proton and neutron densities of the ground state, the nuclear rms radii and elastic form factors of one neutron ^{23}O and ^{24}F halo nuclei were studied by the two body model of $(core + n)$ within the HO and WS radial wave functions. In addition, the Glauber model at high energies has been used to calculate the matter rms radii and reaction cross section (σ_R) of these nuclei.

For the ^{23}O and ^{24}F halo nuclei, the calculations were performed adopting a ^{22}O and ^{23}F cores, respectively, plus single valence neutron for the structure of these nuclei. The core configurations, half-life time and separation energy (S_n) [20, 21] for the studied nuclei are listed Table 1.

The halo (valence) neutron in ^{23}O and ^{24}F was considered to have mixed configuration of $1d_{3/2}$ and $2s_{1/2}$ using the following relation [22]:

$$\rho_v = \left\{\alpha \left|\phi_{2s_{1/2}}\right|^2 + (1-\alpha)\left|\phi_{1d_{3/2}}\right|^2\right\} \quad (\alpha \leq 1)$$

where $\phi_{2s_{1/2}}$ and $\phi_{1d_{3/2}}$ refer to the halo neutron wave functions of $2s_{1/2}$ and $1d_{3/2}$ with occupation probabilities $\alpha = 0.6$ (in $2s_{1/2}$) and $\alpha = 0.4$ (in $1d_{3/2}$) for the halo neutron, respectively and α refer to the occupation probability of the ($2s_{1/2}$) orbital.

The WS parameters for stable nuclei (^{18}O, ^{19}F) and the depth of WS potential (V_0) for core nucleons (protons and neutrons) as well as the depth of spin-orbit (V_{so}) of halo nuclei ^{23}O and ^{24}F were taken from Brown and Rae [23]. The V_0 for outer neutron and the parameters (r_0, r_{so}, a_0 and a_{so}) were adjusted to reproduce the experimental S_n of the outer neutron and the experimental matter rms radii. The parameters of the WS and HO parametrizations used in the present analysis are listed in Table 2.

The calculated rms radii obtained by the two density parameterizations and the corresponding experimental data are summarized in Tables 3 and 4 along with the available calculated results obtained from the relativistic mean field (RMF) method [25]. From the results shown in these tables, it can be clearly seen that the rms radii obtained by the two density parameterizations are consistent with the experimental data more than those of RMF method.

Table 1: Some features for the considered nuclei.

Halo Nucleus	(J^{π}, T) [20]	Half-life time $(\tau_{1/2})$ [20]	S_n (MeV) [21]	Core configuration
^{23}O	$1/2^{+}, 7/2$	$97\ ms$	$S_n = 2.73$	$\{(1s_{1/2})^4, (1p_{3/2})^8, (1p_{1/2})^4, (1d_{5/2})^6\}$
^{24}F	$3^{+}, 3$	$384\ ms$	$S_n = 3.81$	$\{(1s_{1/2})^4, (1p_{3/2})^8, (1p_{1/2})^4, (1d_{5/2})^7\}$

Table 2: Parameters of the WS and HO parametrizations used in the present analysis.

Nuclei	V_0 (MeV)			V_{so} (MeV)	$a_0 = a_{so}$ (fm)	$r_0 = r_{so}$ (fm)	r_c (fm)	b (fm)	
	Core	Valence							
		$1d_{3/2}$	$2s_{1/2}$					b_c	b_v
^{23}O	60.815	36.260	28.280	6.0	0.935	1.375	1.371	1.92	3.62
^{24}F	68.262	34.88	27.94	6.0	0.875	1.395	1.366	1.83	3.60
^{18}O	52.421			6.0	0.645	1.345	1.399	1.799	
^{19}F	62.515			6.0	0.538	1.282	1.392	1.758	

Table 3: Proton and neutron rms radii for the selected nuclei.

Nuclei	$\langle r_p^2 \rangle^{1/2}$(fm)		$\langle r_n^2 \rangle^{1/2}$(fm)		$\langle r_n^2 \rangle_{exp}^{1/2}$(fm) [24]
	WS	HO	WS	HO	
^{23}O	2.78	2.88	3.42	3.55	3.58 ± 0.05
^{24}F	2.79	2.76	3.29	3.42	3.29 ± 0.09

Table 4: Core and matter rms radii for the selected nuclei.

Halo nuclei	$\langle r_{core}^2 \rangle^{1/2}$(fm)		$\langle r_{core}^2 \rangle^{1/2}$ RMF [25]	$\langle r_{core}^2 \rangle_{exp}^{1/2}$ (fm) [24]	$\langle r_m^2 \rangle^{1/2}$ (fm)		$\langle r_m^2 \rangle^{1/2}$ RMF [25]	$\langle r_m^2 \rangle_{exp}^{1/2}$ (fm) [24]
	WS	HO			WS	HO		
^{23}O	2.98	3.09	2.92	3.02±0.05	3.21	3.33	2.98	3.30±0.03
^{24}F	2.91	2.96	2.85	2.93±0.04	3.12	3.21	2.94	3.17±0.05

Fig. 1 presents the calculated matter (dashed-red curve), core (green curve) and halo (dark-blue curve) densities as well as the experimental data of matter densities (shaded region) [26] for ^{23}O (upper part) and ^{24}F (bottom part). The left and right panels correspond to the calculated results obtained by WS and HO parameterizations, consecutively. It is noted that, the calculated results obtained by the two density parameterizations give a good description of the experimental data and show halo component in the matter distributions. Moreover, the dashed-red curves in Figs.1 (a and c) better describs the experimental data than those in Figs. 1 (b and d).

The calculated matter (dashed-red curve), proton (green curve) and neutron (dark-blue curve) densities for ^{23}O and ^{24}F obtained with two density parameterizations are plotted in Fig. 2. It is evident from this figure that there is neutron halo in ^{23}O and ^{24}F as their neutron density distributions have a long tail.

In Fig. 3 the density distribution of matter for unstable exotic ^{23}O and ^{24}F nuclei are compared with those for their stable ^{18}O and ^{19}F isotopes. In the figure, the dashed-red and dark-blue curves are the density distributions of matter for unstable and stable nuclei, consecutively. It is noted that the matter density distributions for each pair of isotopes are different. The weak binding of the outer neutron in exotic ^{23}O and ^{24}F nuclei leads to extended their matter density distributions.

It is clear from Figs.1-3 that the behavior of the matter density in WS and HO parameterizations are diverse because different wave functions that used in these two parameterizations.

The elastic form factors of exotic ^{23}O and ^{24}F nuclei (red curves) calculated by PWBA using the WS and HO proton densities are compared in Fig. 4 with those for their stable ^{18}O and ^{19}F isotopes (dark-blue curves) together with the experimental data (dark-blue symbol) of stable isotopes [27, 28]. It is noted that the form factors for each isotopes pairs are quite different although they have the same proton number. The minima position of the red curve has shifted to the left as compared with that of the dark-blue curve. This change is attributed to the variation in the proton densities due to the presence of the extra neutrons.

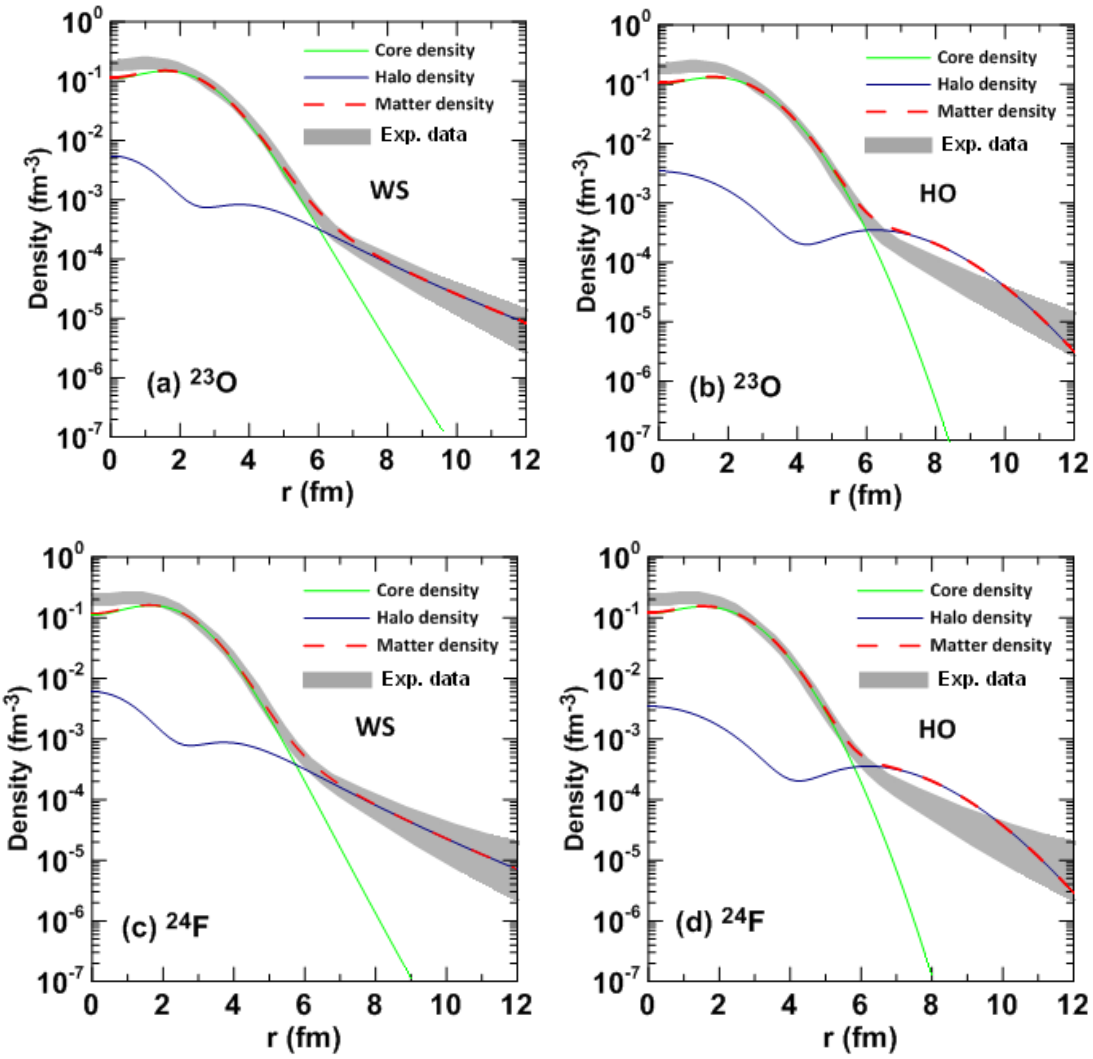

Fig.1: The matter, core and halo densities for halo nuclei ^{23}O and ^{24}F.

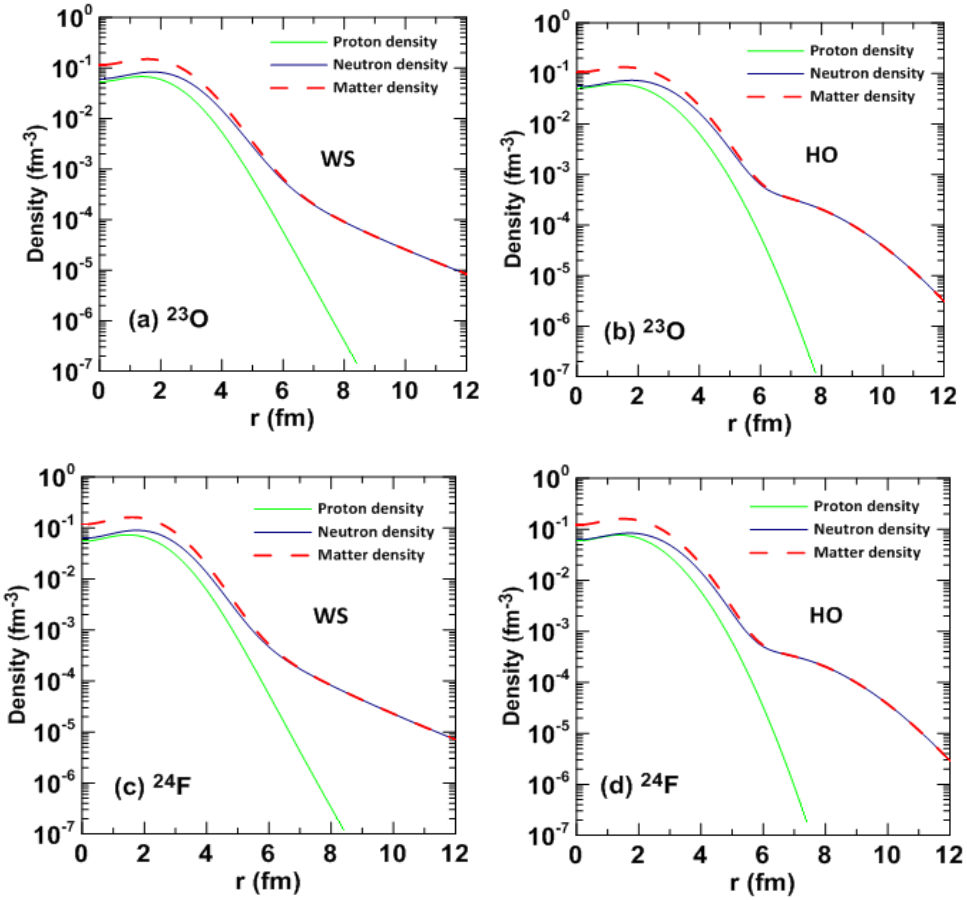

Fig.2: The matter, proton and neutron densities for halo nuclei ^{23}O and ^{24}F.

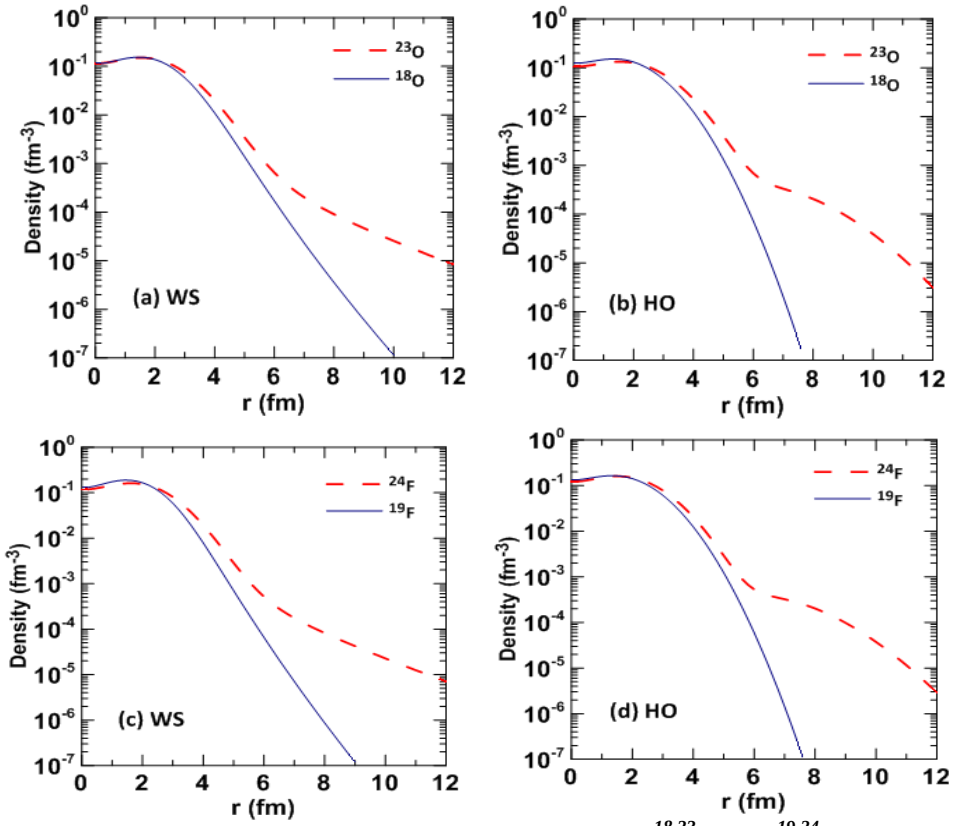

Fig. 3: Calculated matter densities for nuclei ^{18,23}O and ^{19,24}F.

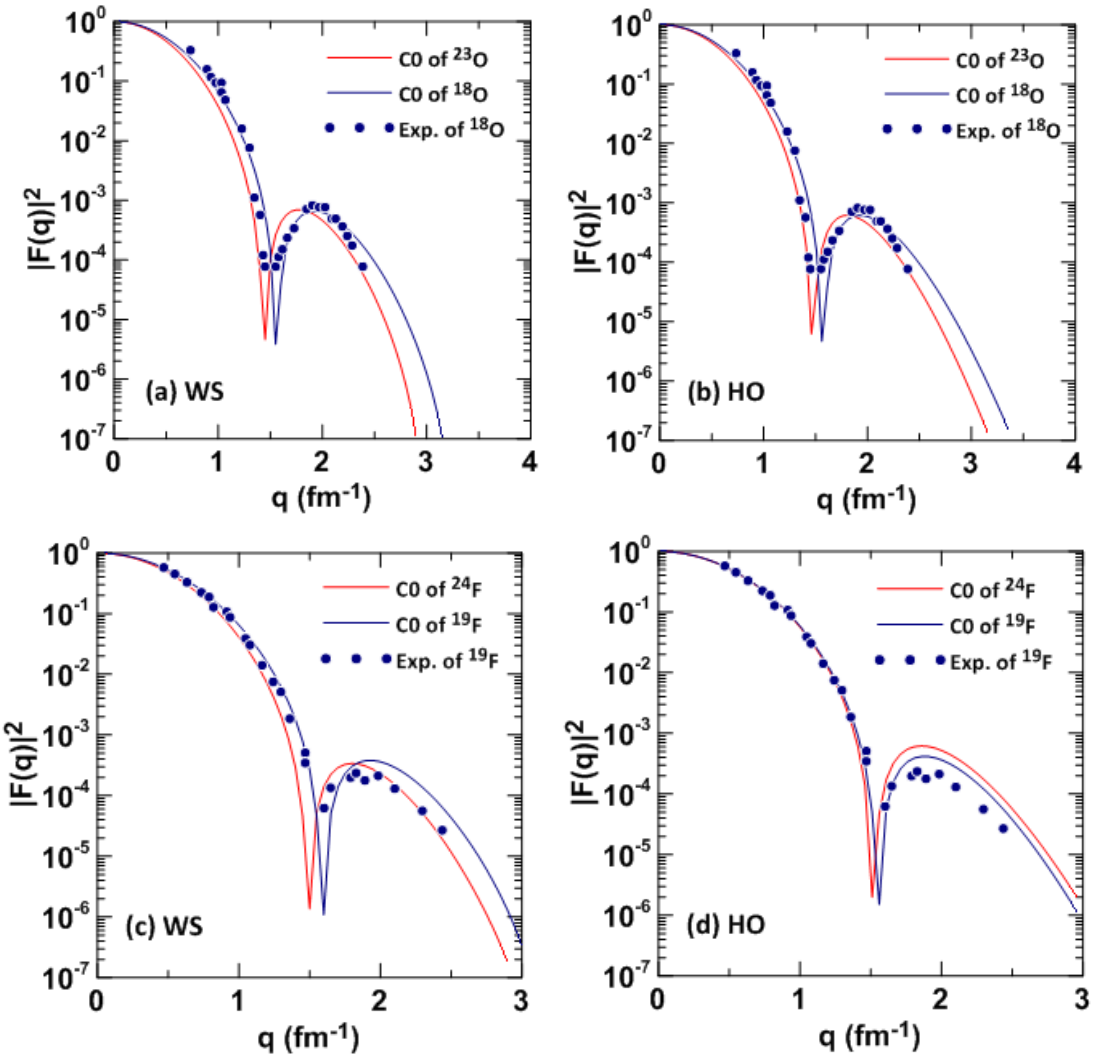

Fig.4: Elastic form factors for nuclei ^{18,23}O and ^{19,24}F.

The calculated σ_R at high energy for ^{23}O + ^{12}C and ^{24}F + ^{12}C systems using the Glauber model with OLA along with experimental data are listed in Table 5. From the results shown in Table 5, it can be clearly seen that a good description of the experimental σ_R is obtained by the calculated results for both halo nuclei.

Table 5: Calculated and experimental σ_R for ^{23}O + ^{12}C and ^{24}F + ^{12}C systems.

Halo nuclei	Energy (MeV) [24]	Calculated σ_R (mb)	Experimental σ_R (mb) [24]
^{23}O	960	1312	1308±16
^{24}F	1005	1257	1253±23

To calculate the matter rms radius of halo nuclei from the reaction cross sections (σ_R), the calculated σ_R (red line) obtained by the Glauber model within OLA versus the matter rms radii for the halo nuclei ^{23}O and ^{24}F on ^{12}C target at high energy are plotted in Figs.5 (a and b), consecutively. The horizontal black line shows the experimental σ_R (given in Table 5) with error bar plotted by the shaded area. The intersection point of the red line with horizontal black line represents the obtained matter rms radius ($\langle r_m^2 \rangle^{1/2}$) for the halo nuclei. From Fig.5(a) [Fig.5(b)] the calculated

$\langle r_m^2 \rangle^{1/2}$ for ^{23}O [^{24}F] is equal to 3.28 [3.04] fm which agrees well with the analogous experimental data of the value 3.30±0.03 [3.17±0.05] fm.

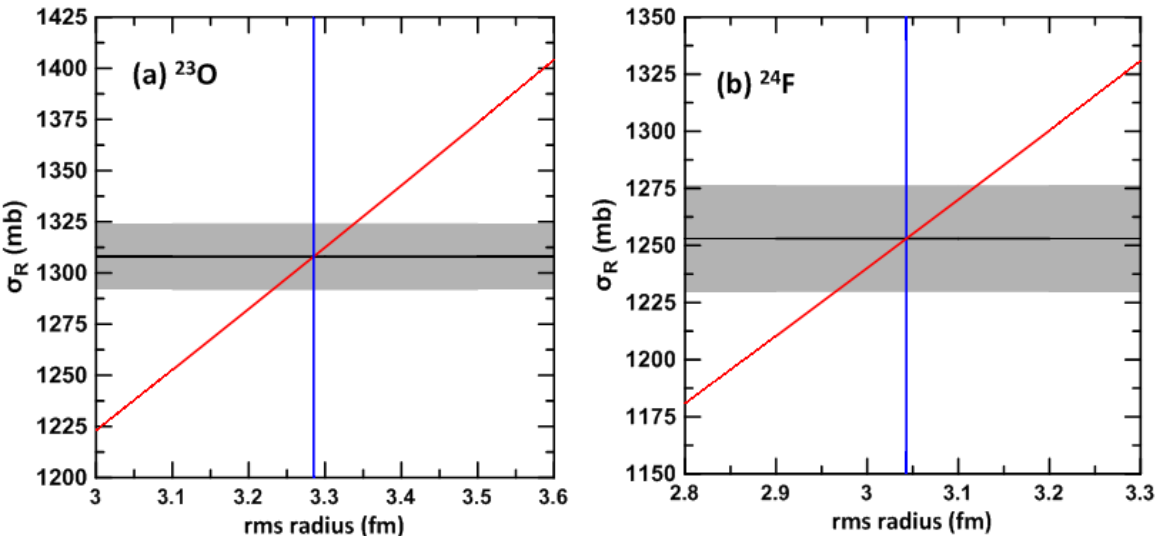

Fig.5: The reaction cross section versus the matter rms radii for the halo nuclei ^{23}O and ^{24}F.

Conclusions

From this study the following conclusions can be drawn:

1- It was found that the two body model of $(core + n)$ within the HO and WS radial wave functions is remarkably capable of providing theoretical predictions on the structure of halo nuclei and be in a satisfactory description with those of experimental data.

2- The halo structure of one neutron ^{23}O and ^{24}F exotic nuclei was emphasized through exhibiting the long tail performance in their calculated neutron and matter density distributions, where this performance is considered as a distinctive feature of halo nuclei.

3- The results of the matter density distributions calculations when the halo neutron in ^{23}O and ^{24}F has mixed configuration of $(1d_{3/2})$ and $(2s_{1/2})$ with dominant $(2s_{1/2})$ were in best agreement with experimental data.

4- It was found that the major difference between the calculated form factor of unstable nuclei ^{23}O and ^{24}F and those of their stable isotope ^{18}O and ^{19}F can be attributed to the variation in the proton densities due to the presence of the extra neutrons.

5- The Glauber model at high energy gave a good description for both matter rms radii and σ_R of these nuclei.

References

[1] I. Tanihata, J. Phys. G: Nucl. Part. Phys., 22 (1996) 157-198.

[2] P.G. Hansen, A.S. jensen, B. Jonson, Ann. Rev. Nucl. Part. Sci., 45 (1995) 591-634.

[3] B. Q. Chen, Z. Y. Ma, F. Grümmerd, S. Krewald, J. Phys. G: Nucl. Part. Phys., 24, 1 (1998) 97-105.

[4] Z. Ren, A. Faessler, A. BobykPhys. Rev., C 57 (1998) 2752-2755.

[5] R. Morlock, R. Kunz, A. Mayer, M. Jaeger, A. Müller, J. W. Hammer, P. Mohr, Phys. Rev. Lett., 79 (1997) 3837-3840.

[6] A. Navin, D. Bazin, B. A. Brown, B. Davids, G. Gervais, T. Glasmacher, K. Govaert, P. G. Hansen, M. Hellström, Phys. Rev. Lett., 81 (1998) 5089-5092.

[7] C. B. Qiu and M. Z. Yu, Chin. Phys. Lett., 18, 12 (2001) 1561-1563.

[8] Zhao, Yao-Lin, Ma, Zhong-Yu, Chen, Bao-Qiu, Shen, Wen-Qing, Chin. Phys. Lett., 20 (2003) 53.
[9] A. Y. A. Alsajjad and A. N. Abdullah, Diyala Journal for Pure Science, 15, 4 (2019) 120-136.
[10] A. N. Abdullah, Int. J. Mod. Phys., E 26, 7 (2017) 1750048-1_1750048-11.
[11] A. N. Abdullah, Int. J. Mod. Phys., E 29, 3 (2020) 2050015-1_2050015-10.
[12] A. N. Abdullah, Mod. Phys. Lett., A 35 (2020) 2050212.
[13] W. Meng, Chin. Phys. C 32 (2008) 548-551.
[14] Y. Chu, Z. Z. Ren and C. Xu, Eur. Phys. J., A 37 (2008) 361–366.
[15] P. J. Brussard and P. W. M. Glaudemans, "Shell-Model Application in Nuclear spectroscopy", North-Holland, Amesterdam (1977).
[16] L. G. Qiang, J. Phys. G. Nucl. Part. Phys., 17 (1991) 1-34.
[17] A. N. Antonov, M. K. Gaidarov, D. N. Kadrev, P. E. Hodgson, E. Moya De Guerra, Int. J. Mod. Phys. E 13, 4 (2004) 759-772.
[18] T. Zheng, T. Yamaguchi, A. Ozawa, M. Chiba, R. Kanungo, Nucl. Phys., A 709 (2002) 103-118.
[19] J. A. Tostevin, J. S. Al-Khalili, Nucl. Phys., A 616 (1997) 418c-425c.
[20] M. Wang, G. Audi, F.G. Kondev, W.J. Huang, S. Naimi, Xing Xu, Chin. Phys., C 41 (2017) 030003.
[21] G. Audi, F.G. Kondev, Meng Wang, W.J. Huang, S. Naimi, Chin. Phys., C 41, 3 (2017) 030001.
[22] F. D. Qing, Chun-wang Ma, Yu-Gang Ma, Xiang-Zhou Cai, Jin-Gen Chen, Chin. Phys., C 22, 3 (2005) 572-575.
[23] B. A. Brown and W. D. M. Rae, Nucl. Data Sheets, 120 (2014) 115-118.
[24] Suhel Ahmad, A. A. Usmani, Z. A. Khan, Phys. Rev., C 96 (2017) 064602.
[25] J.S. Wang, W.Q. Shen, Z.Y. Zhu, J. Feng, Z.Y. Guo, Nucl. Phys., A 691 (2001) 618-630.
[26] A. Ozawa, Eur. Phys. J. A 13 (2002) 163-167.
[27] R. Kuchta, Phys. Rev., C 38 (1988) 1460-1474.
[28] P. L. Hallowell, W. Bertozzi, J. Heisenberg, S.Kowalski, X.Maruyama, C.P. Sargent, W. Turchinetz, C.F. Williamson, S.P. Fivozinsky, J.W. Lightbody, Jr., S. Penner, Phys. Rev., C 7 (1973) 1396-1409.